Available online at www.sciencedirect.com
SCIENCE DIRECT®
ELSEVIER
Icarus 172 (2004) 9–23
ICARUS
www.elsevier.com/locate/icarus

Life cycles of spots on Jupiter from Cassini images

Liming Li [a,*], Andrew P. Ingersoll [a], Ashwin R. Vasavada [b], Carolyn C. Porco [c], Anthony D. Del Genio [d], Shawn P. Ewald [e]

[a] *Division of Geological and Planetary Sciences, MS 150-21, California Institute of Technology, Pasadena, CA 91125, USA*
[b] *Department of Earth and Space Sciences, University of California Los Angeles, Los Angeles, CA 90095, USA*
[c] *Southwest Research Institute, Boulder, CO 80302, USA*
[d] *NASA Goddard Institute for Space Studies, Broadway, New York, NY 10025, USA*
[e] *Division of Geological and Planetary Sciences, California Institute of Technology, Pasadena, CA 91125, USA*

Received 12 February 2003; revised 24 September 2003

Available online 20 December 2003

Abstract

Using the sequence of 70-day continuum-band (751 nm) images from the Cassini Imaging Science System (ISS), we record over 500 compact oval spots and study their relation to the large-scale motions. The ∼ 100 spots whose vorticity could be measured—the large spots in most cases—were all anticyclonic. We exclude cyclonic features (chaotic regions) because they do not have a compact oval shape, but we do record their interactions with spots. We distinguish probable convective storms from other spots because they appear suddenly, grow rapidly, and are much brighter than their surroundings. The distribution of lifetimes for spots that appeared and disappeared during the 70-day period follows a decaying exponential with time constant (mean lifetime) of 3.5 days for probable convective storms and 16.8 days for all other spots. Extrapolating the exponential beyond 70 days seriously underestimates the number of spots that existed for the entire 70-day period. This and other evidences (size, shape, distribution in latitude) suggest that these long-lived spots with lifetime larger than 70 days are from a separate population. The zonal wind profile obtained manually by tracking individual features (this study) agrees with that obtained automatically by correlating brightness variations in narrow latitude bands (Porco et al., 2003). Some westward jets have developed more curvature and some have developed less curvature since Voyager times, but the number of westward jets that violate the barotropic stability criterion is about the same. In the northern hemisphere the number of spots is greatest at the latitudes of the westward jets, which are the most unstable regions according to the barotropic stability criterion. During the 70-day observation period the Great Red Spot (GRS) absorbed nine westward-moving spots that originated in the South Equatorial Belt (SEB), where most of the probable convective storms originate. Although the probable convective storms do not directly transform themselves into westward-moving spots, their common origin in the SEB suggests that moist convection and the westward jet compose a system that has maintained the GRS over its long lifetime.

Keywords: Atmospheres, dynamics; Jupiter, atmosphere; Meteorology

1. Introduction

Jupiter's atmosphere is full of spots—compact, oval-shaped cloud features whose appearance, at some wavelengths at least, is different from that of their surroundings. This contrast may reflect differences in composition or size of the cloud particles, differences in optical thickness or altitude of the cloud, or differences in small-scale texture of the cloud (Smith et al., 1979; Ingersoll et al., 1979; Mitchell et al., 1979). Some spots have lightning in them, as revealed in night side images (Little et al., 1999; Gierasch et al., 2000).

Spots form in a variety of ways (Mac Low and Ingersoll, 1986). Some gather contrast slowly in an otherwise featureless region; some develop coherence and emerge from the turbulent flow; and others appear suddenly as bright points and grow by expansion. Likewise, some spots are absorbed by the turbulent flow; some are destroyed by mergers; and others simply fade away. "Life cycles" refers to appearances and disappearances, mutual interactions, and interactions with the zonal jets. Comparing the observed life cycles with

* Corresponding author.
E-mail address: liming@gps.caltech.edu (L. Li).

0019-1035/$ – see front matter
doi:10.1016/j.icarus.2003.10.015

those produced in numerical models (e.g., Ingersoll and Cuong, 1981; Williams and Yamagata, 1984; Marcus, 1988; Dowling and Ingersoll, 1989) leads to a better understanding of the dynamics of Jupiter's atmosphere.

Our study uses data spanning 70 days (October 1 to December 9, 2000) of observation by the Cassini Imaging Science System (ISS) in a filter centered at 751 nanometers. The only other comparable study (Mac Low and Ingersoll, 1986) used 58 days of observation by the Voyager imaging system in the violet filter. In both cases the resolution of the raw images ranged from ~ 500 km/pixel at the beginning of the sequence to ~ 100 km/pixel at the end. Voyager imaged the disk of the planet every 1/5 of a jovian rotation and covered the entire planet once per jovian rotation, i.e., once every 10 h. The mosaics became a movie with time step ~ 10 h and duration ~ 58 Earth days. Cassini operated in much the same way, except it often skipped a rotation so that the time step was sometimes 10 h and sometimes 20 h. Morales-Juberias et al. (2002), hereinafter MJ, studied spots using HST data over a 6-year period. The temporal sampling is less dense than ours, but we will compare our results with theirs wherever possible.

Each Cassini image was navigated by fitting (in the image plane) the observed planetary limb to its predicted location. Radiometric calibration was performed using the CISSCAL software developed by the Cassini ISS Team. The images for each rotation were projected into a simple cylindrical map spanning 360° of longitude. Illumination effects were removed by dividing by the cosine of the incidence angle, and regions shared by multiple images were averaged. The final maps were converted to 8-bit images using the same linear stretch for all maps and are stored without compression. To date, these steps have been performed for the 751 nm filter only, although raw images spanning the same 70-day period exist for several other filters.

Each Cassini mosaic is 3600×1801 pixels and spans 360° of longitude and 180° of latitude. Therefore each pixel spans 0.1° of longitude and 0.1° of latitude. The scale of 0.1°/pixel, or ~ 125 km/pixel at the equator, was chosen such that all the 70-day images could be mapped consistently without loss of information. The spatial areas over which spots are measured include all 360° in longitude and 80° S to 80° N in latitude. The gases in Jupiter's troposphere are transparent in the 751-nm band, so these near-infrared continuum band images can capture a multitude of spots at different altitudes in the troposphere of Jupiter.

We use the term "spot" to describe a structure having the following four characteristics:

(1) compact oval shape,
(2) appearance in at least three successive images (life–history at least 40 h),
(3) a marked brightness difference from the surrounding clouds,
(4) diameter at least 700 km during some part of the spot's life.

According to this definition, we record over 500 spots. We observe the sign of the vorticity for about 100 of the largest spots, whose rotation direction can be determined from a movie made from these images, and find that all these spots are anticyclonic (clockwise in the northern hemisphere, counterclockwise in the southern hemisphere). Among the 517 compact spots we record, 306 compact spots are bright and 211 compact spots are dark. The dark spots may be holes in the clouds or they may be dark cloud material that absorbs the light at 751 nm. Other studies (Banfield et al., 1998) suggest that bright and dark contrast originates at ~ 0.7 bar. We use planetographic latitudes, system III west longitudes, and positive zonal winds in the eastward direction. Mac Low and Ingersoll (1986) recorded over 100 spots in the Voyager mosaics. Their study focused on interactions between spots. Our study is larger (500 vs 100 spots) and more general; it includes appearances, disappearances, distribution of lifetimes, size distribution, mutual interactions, interactions with the Great Red Spot (GRS), distribution with respect to latitude, and motion relative to the zonal jets.

We use the term chaotic region (CR) to define a patch of rapidly changing, amorphous features. CR's are distinct from compact spots, and are not included in our study except as they interact with spots. In many cases it is difficult to define the boundaries of a CR, and in some cases a CR is simply a cyclonic band circling the entire planet. Smith et al. (1979) called these patches "disturbed regions." Ingersoll et al. (1979) and Mitchell et al. (1979) used the term "turbulent, folded-filament regions." They also used the term "oblong cyclones," since the vorticity of the CR's is always cyclonic. These authors used the term "wakelike" to describe the CR's to the west of the large ovals. The largest wakelike region is the South Equatorial Belt (SEB) to the west and slightly equatorward of the Great Red Spot (GRS). Youssef and Marcus (2003) point out that a row of cyclonic CR's alternating with a row of anticyclonic ovals resembles a Karman vortex street. With a numerical model they show that the relative positions of the vortices are stable. In a classic vortex street the cyclones and anticyclones have the same size. On Jupiter the east–west dimension of the CR's is usually greater than that of the associated ovals.

2. Appearances and disappearances

Figure 1 shows that the number of appearances minus disappearances oscillates around zero. Over the whole period the numbers of appearances (393) and disappearances (356) are basically in balance, and their difference $(393 - 356 = 37)$ is not statistically significant. The null hypothesis is that both appearances and disappearances in a 70-day period have a mean of $374.5 = (393 + 356)/2$. The standard deviation of each is $374.5^{1/2} = 19.4$. The standard deviation of their difference is $(2 \times 374.5)^{1/2} = 27.4$. The actual difference is 37, which is 1.35 standard deviations and not statistically significant.

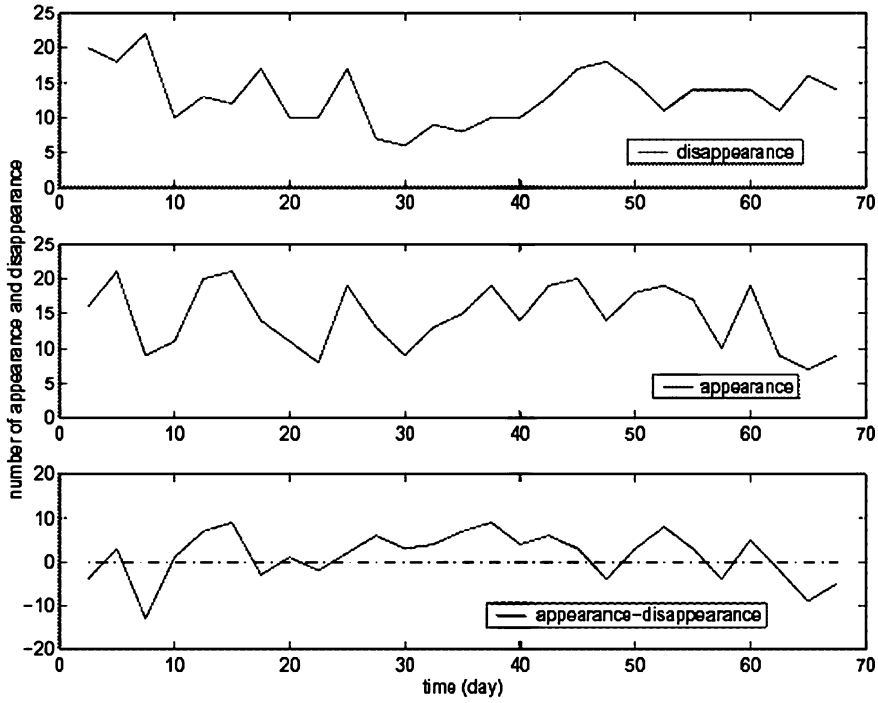

Fig. 1. The numbers of appearances and disappearances of spots every 60 h during the 70-day period. The figure also shows the value of appearance minus disappearance during the period.

Mac Low and Ingersoll (1986) observed 23 mergers, 23 other kinds of disappearances, and 19 appearances, roughly an order of magnitude fewer events than in our study. These authors noted that the number of spots destroyed was a factor of 2 greater than the number created during the 58-day observation period, and recommended further study of the budget. However, the main goal of their paper was to study the time-dependent behavior of interacting spots. The appearance of a spot is a solitary event. The fact that they observed less than one appearance per day whereas we observed more than four appearances per day suggests that Mac Low and Ingersoll did not record most of those events. In the long run, the appearance and disappearance of spots should be in balance.

We divide appearances into three types:

(1) development of contrast in an otherwise featureless region,
(2) development of a coherent structure in an otherwise turbulent region,
(3) sudden appearance of a bright point followed by rapid expansion in size.

Type 1 usually takes place outside the CR's, whereas types 2 and 3 usually take place in the CR's. Type 2 often involves ejection of the spot from a CR. Type 3 describes the rapidly growing, easily identified features that often have lightning in them (Little et al., 1999; Gierasch et al., 2000; Ingersoll et al., 2000). Porco et al. (2003) referred to these as "convective storms" in their analysis of the Cassini data. However, neither Porco et al. (2003) nor we observed the lightning directly, so we will call them "probable convective storms." The resolution in our images ranges from 100 to 500 km, which is enough to resolve the probable convective storms in the SEB (10° S–16° S) and the NEB (10° N–15° N). Compared with Porco et al. (2003) we did not find many convective storms at other latitudes, probably because we used just the 751 nm filter and they used other filters including those in the strong and weak methane bands. Convective storms are important for the jovian atmosphere because they can transport much of the heat flux from the deeper troposphere (Gierasch et al., 2000).

Figure 2a displays an example of a spot developing in a relatively calm area (type 1). This is the most frequent kind of appearance among the three types (221 out of 393 cases). The gradual appearance of the spot in Fig. 2a is not due to the change in resolution, because in the first two subimages we can see that the embryo did not have elliptical shape and we can see much smaller scale features than the embryo itself. Figure 2b shows a spot that emerged from the turbulence in a CR (type 2). This is the next most frequent kind of appearance (141 out of 393). Figure 3a shows a very bright spot that grows rapidly (type 3), and is probably a convective storm. This is the least frequent kind of appearance (31 out of 393 cases).

We also divide disappearances into three types:

(1) disappearance due to merging,
(2) destruction by the turbulence, usually in a CR,
(3) gradual fading.

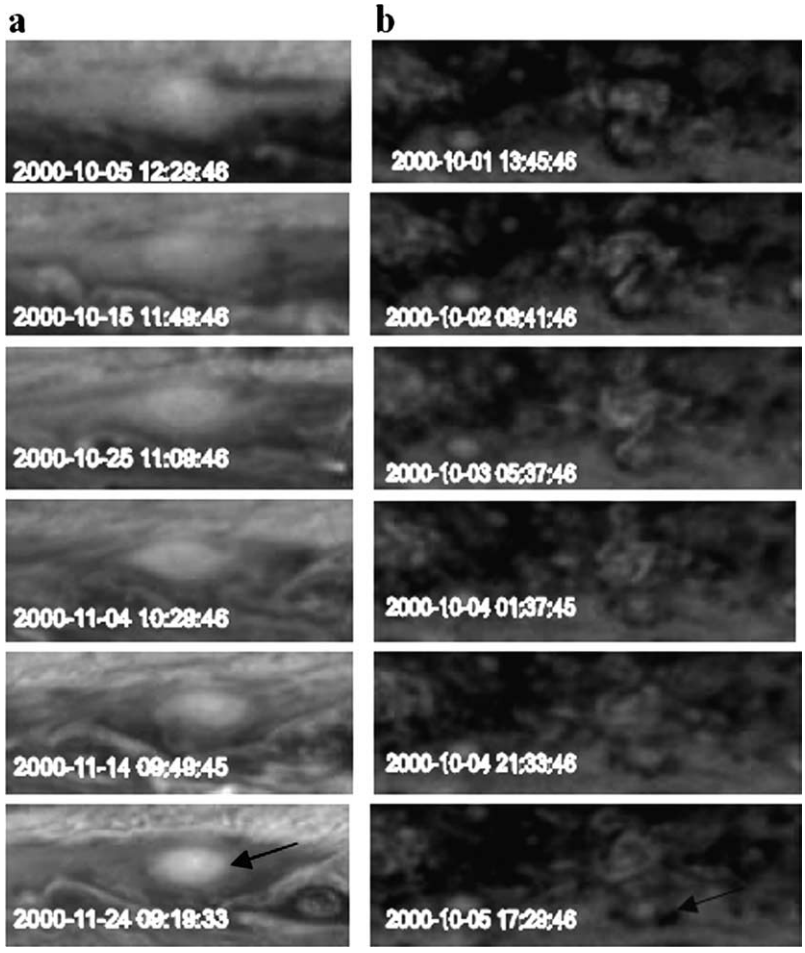

Fig. 2. (a) Large spot developing slowly outside of a CR. In this figure and all other figures like it (Figs. 2b, 3a, 3b, 4a, and 4b), time increases from top to bottom. Note that the time step between neighboring subimages of Fig. 2a is 10 days, so the spot is developing very slowly. The time step for all other such figures (Figs. 2b, 3a, 3b, 4a, and 4b) is 20 h. The range for every frame of Fig. 2a is (12° N–23° N, 350°–17°). The time of the first subimage (the top one) is Oct 5, 2000. The large spot covers the center of the 17° N westward jet. (b) Spot coming from a CR. The range for every frame is (42° N–54° N, 230°–267°). The time of the first subimage is Nov 5, 2000. The spot sits in an anticyclonic band.

Figure 3b shows a merger between two spots. This type of disappearance is different from destruction by turbulence (Fig. 4a) because it results in a recognizable spot. Absorption by turbulence results in more turbulence—amorphous, rapidly changing patterns that have no definite spots. Mac Low and Ingersoll (1986) were especially interested in mergers because the solitary wave model (Maxworthy et al., 1978) predicted that when one spot overtakes another at the same latitude they would pass through each other, whereas other models (Ingersoll and Cuong, 1981; Williams and Yamagata, 1984) predicted that the two spots would merge. We record 119 mergers and 7 near misses—where spots passed around each other—out of the total 126 interactions during the 70-day period. Our result seems to support these merging models.

Figure 4a shows a small spot that is destroyed by turbulence inside a CR. This kind of disappearance accounts for more than one-fourth of the total number of disappearances (90 out of 356). CR's are not only an important source of spots but also an important sink of spots. Figure 4b shows a spot that fades away. It disappears without undergoing any interaction with other spots or CR's. The number of this kind of disappearance is largest among the three types of disappearance (147 out of 356 cases).

3. Dimensions

In Fig. 5 we record the sizes of all spots and give a scatter plot of north–south (NS) and east–west (EW) diameters based on the brightness and lifetime. In our study, long-lived spots are those that existed throughout the entire 70-day period, and short-lived spots are those that both appeared and disappeared during the 70-day period. The GRS and white oval at −33° are not included in the list of long-lived spots. Figure 5 offers two different linear fits between the two diameters by assuming that the uncertainties of measurement in major and minor diameters are the same (Meyer, 1986). The fitting lines from the origin indicate that long-lived spots and dark spots have smaller NS/EW ratios than short-lived

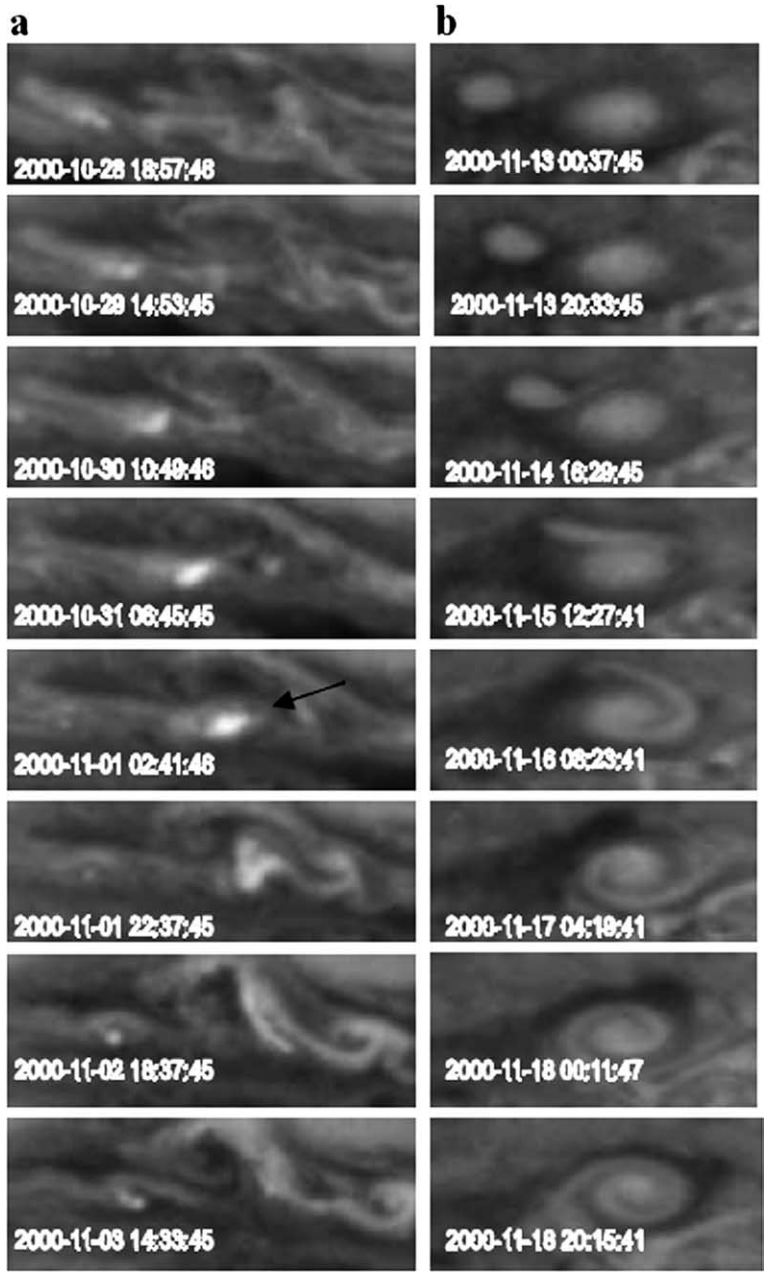

Fig. 3. (a) A fast-developing spot in a CR, probably a convective storm. The range for every frame is (9° N–17° N, 8°–30°). The time of the first subimage is Oct 29, 2000. The spot sits in a cyclonic band. (b) Two spots merging with each other. The range for every frame is (38° N–45° N, 280°–295°). The time of the first subimage is Nov 13, 2000. The two spots sit in an anticyclonic band.

spots and bright spots. The two-parameter fit presents a different result because it is more sensitive to spots having extreme low and high ratios than the fit from the origin.

Figure 5 shows that all the long-lived spots have major diameters greater than ~ 2000 km. The short-lived spots have major diameters ranging from below 1000 to over 6000 km. There is no correlation between lifetime and size for the short-lived spots, and we cannot measure the lifetimes of the long-lived spots. Our results are generally in agreement with Figs. 4 and 6 of MJ, although our study has a smaller minimum spot size (700 vs 1500 km) and a shorter time base than theirs.

4. Distribution of lifetimes

The time between the appearance and disappearance of a spot is its lifetime. Figure 6 is a histogram of lifetimes, constructed using those spots having a complete life history during Cassini's 70-day observation window. The histogram has a bias, which is correctable: A spot with lifetime $t < 70$ days must appear in the initial $(70 - t)$ days of the observation window to be included in the histogram. Spots with lifetimes $t > 70$ days are not included in the histogram. Thus if n_{A} is the average number of spots that appear during a 70 day window and $p(t)\,dt$ is the fraction whose lifetimes

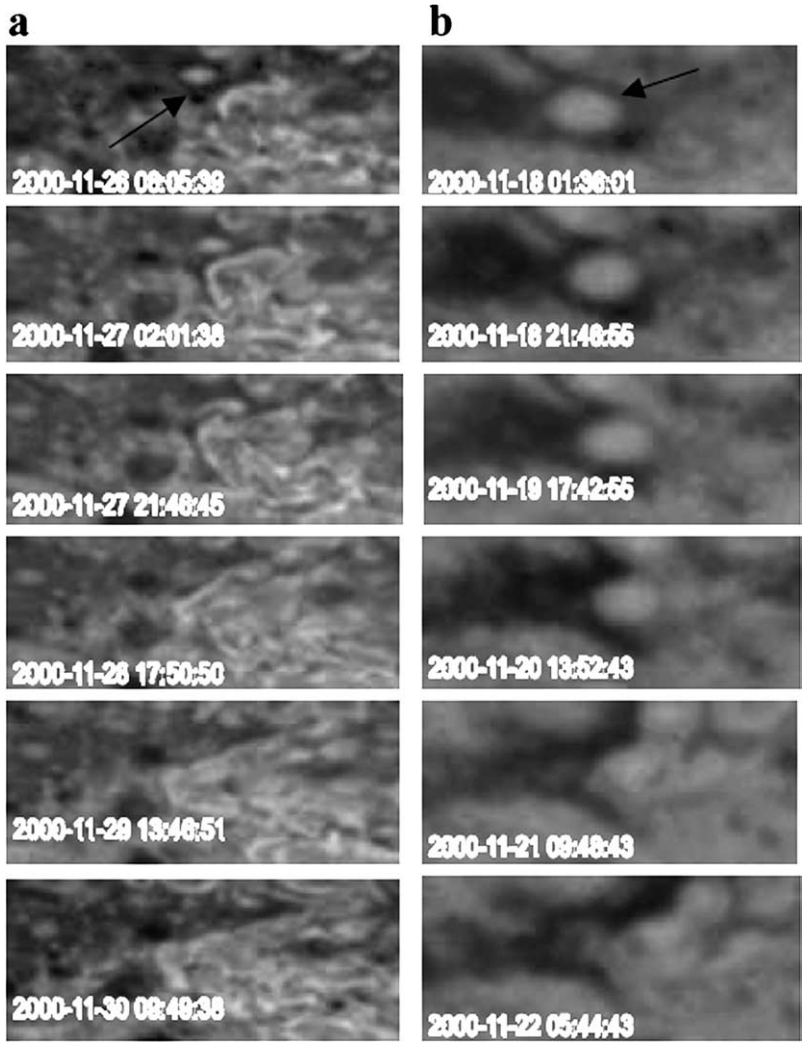

Fig. 4. (a) A small spot destroyed by a CR. The range for every frame is (46° N–57° N, 90°–117°). The time of the first subimage is Nov 25, 2000. The spot sits in an anticyclonic band and meets the left side of a turbulent structure in the CR. (b) A spot that lost contrast and faded away. Sometimes this case resembles that in Fig. 4a, absorption by turbulence. The range for every frame is (42° N–48° N, 310°–324°). The time of the first subimage is Nov 18, 2000. The spot covers the center of the 45° N eastward jet.

are in the range $(t,\ t+dt)$, then $(70-t)/70 n_{\mathrm{A}} p(t)\,dt$ is the number in this lifetime range that appear and disappear in the window. This is the histogram displayed in Fig. 6.

In Fig. 6, the fitted curves show $(70-t)/70 n_{\mathrm{A}} p(t)\,dt$, where $dt = 1$ day and $p(t) = (1/\tau)\exp(-t/\tau)$. For the value of n_{A} we average the number of appearances and the number of disappearances, since the two are the same except for statistical fluctuations. This gives $n_{\mathrm{A}} = 29.5$ for the upper panel and $n_{\mathrm{A}} = 345$ for the lower panel. The one adjustable parameter is τ, and the fitting yields $\tau = 3.5$ days for the probable convective storms and $\tau = 16.8$ days for all other spots. We separated the latter (other spots) into a bright group and a dark group, and fit the distribution of lifetimes for the two groups separately (not shown). The fitting shows that the time constant of bright spots having a complete life history ($\tau = 14$ days) is smaller than the time constant of dark spots having a complete life history ($\tau = 21$ days).

The expectation value for the total number of spots that appear and disappear in the window is

$$n_{\mathrm{AD}} = n_{\mathrm{A}} \int_0^{70} (70-t)/70 p(t)\,dt.$$

The expected number n_{AO} of spots that only appear in the window and disappear later is $n_{\mathrm{A}} - n_{\mathrm{AD}}$. The expected number n_{DO} of spots that only disappear in the window and appear earlier is also $n_{\mathrm{A}} - n_{\mathrm{AD}}$. Actual numbers will be different because of statistical fluctuations.

Information about lifetime $t > 70$ days is contained in the number n_{LL} of long-lived spots that existed throughout the observation period. To be included in this number, a spot with lifetime t must appear no more than $(t-70)$ days before the start of the Cassini observation window. Thus if $n_{\mathrm{A}} p(t)\,dt$ is the average number of spots appearing in a 70 day window with lifetimes in the range $(t,\ t+dt)$, then

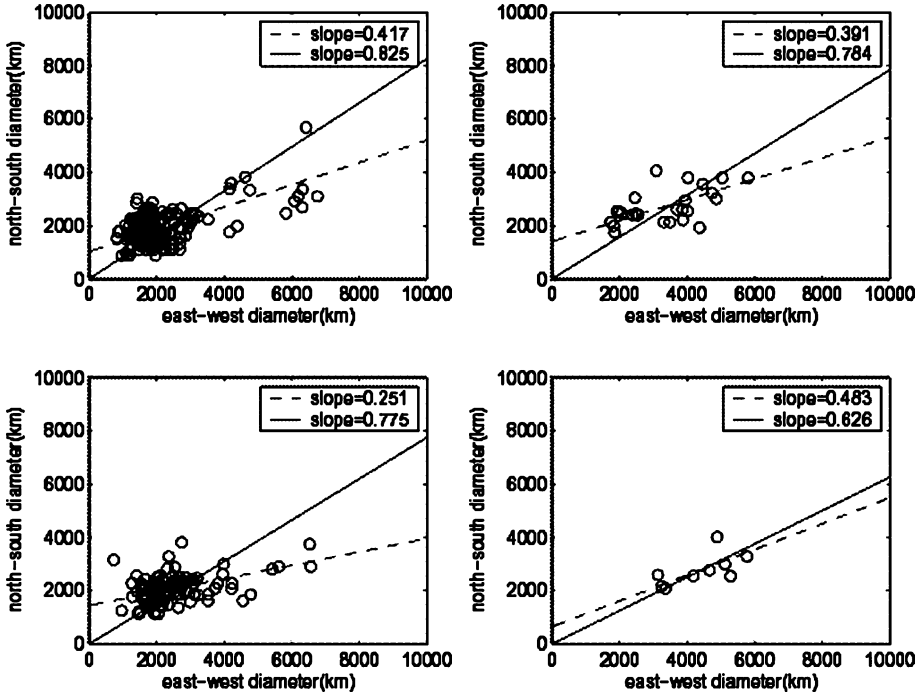

Fig. 5. Scatter plot of the major and minor diameters of spots. The left-top panel is for bright short-lived spots, and the left-bottom panel is for dark short-lived spots. The right-top panel is for bright long-lived spots, and the right-bottom is for dark long-lived spots. Solid lines are one-parameter (slope) linear fitting from origin, and the dashed lines are two-parameter (slope and intercept) linear fitting.

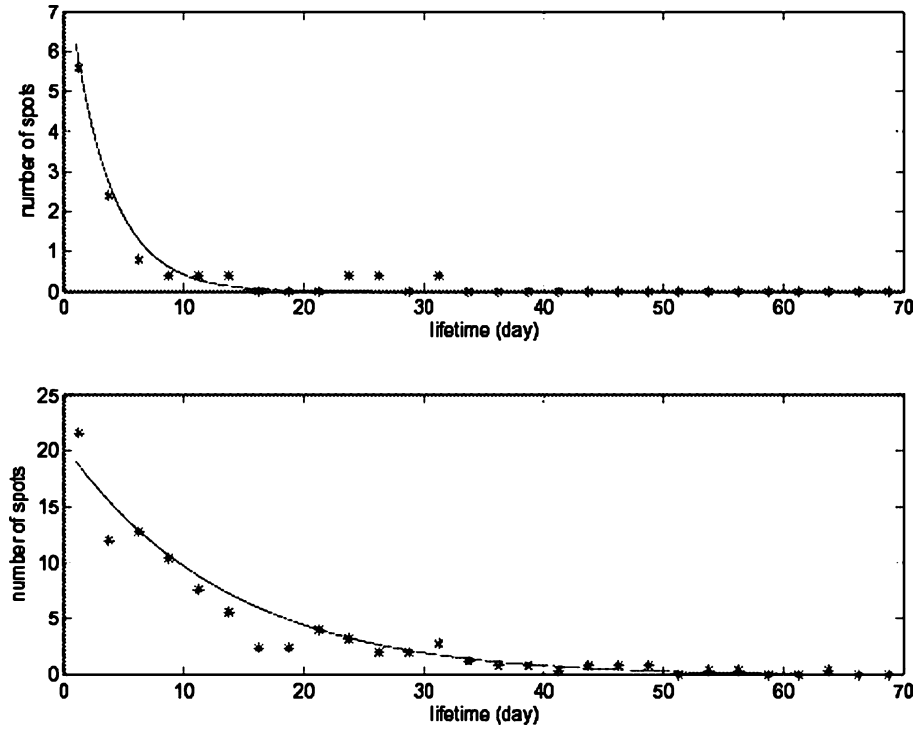

Fig. 6. The distribution of lifetimes of spots having complete life cycles during the 70-day period. Each point represents the average number of spots in a lifetime bin 1 day wide. The upper panel is for probable convective storms and the bottom panel is for all other spots.

$(t-70)/70 n_{\mathrm{A}} p(t)\,dt$ is the number that exist throughout the observation period. The integral is the expectation value of n_{LL}:

$$n_{\mathrm{LL}} = n_{\mathrm{A}} \int_{70}^{\infty} (t-70)/70\, p(t)\, dt.$$

Table 1
Number of appearances and disappearances

	n_{LL}	n_{AO}	n_{DO}	n_{AD}
Probable convective storms (expected)	0	2	2	27
Probable convective storms (observed)	0	3	0	28
All other compact spots (expected)	1	82	82	263
All other compact spots (observed)	35	123	89	239

n_{LL} = long-lived spots, lifetime > 70-days.
n_{AO} = appear only, disappear later.
n_{DO} = disappear only, appeared earlier.
n_{AD} = appear and disappear in the 70-day period.

In Table 1 we compare the observed and expected values of n_{LL}, n_{AO}, n_{DO}, and n_{AD} for probable convective storms and for all other spots. The expected values use the best fit to the histogram in Fig. 6, with $\tau = 3.5$ days for the probable convective storms and $\tau = 16.8$ days for all other spots. The number of appearances is $n_{AO} + n_{AD}$, and the number of disappearances is $n_{DO} + n_{AD}$. Except for n_{LL}, the differences between the observed and expected numbers are consistent with statistical fluctuations. However, the expected number of nonconvective (other) spots that survive for the entire 70-day period is 1, whereas the observed number is 35. Evidently there are more spots with long lifetimes than the exponential distribution would suggest. There is even some evidence that the spots with lifetimes longer than 70 days are from a different population: As shown below, the long-lived spots have different distributions with respect to latitude and size than the spots that appear and disappear in the Cassini observation window.

5. Relation to zonal winds

Much work on zonal winds of Jupiter has been done based on the data sets of Voyager, Galileo, and HST (Ingersoll et al., 1981; Limaye, 1986; Vasavada et al., 1998; Garcia-Melendo and Sanchez-Lavega, 2001). These studies support the idea that the zonal wind profile at the cloud level has remained basically unaltered in spite of some minor variations in jet shape and speed. This implies that the global circulation of Jupiter is stable even though there are turbulence and convection in the atmosphere.

Feature tracking and correlation are two methods for measuring the wind velocity on Jupiter. By manually following the target clouds in images taken at different times, the feature tracking method can determine the wind speed at the latitudes where these target clouds sit, if clouds can be regarded as passive tracers of atmospheric mass motion. For this method, the change of feature shape, the interaction between these clouds and their environment, and operator judgment will cause some errors. On the other hand, the correlation method takes a narrow latitude band spanning 360° in longitude as the target and determines its mean east–west movement by finding the largest correlation coefficient between two images taken at different times. Systematic errors caused by changes of the clouds, wave-like phenomena, and large vortices (GRS, for example) will affect the correlation method (Garcia-Melendo and Sanchez-Lavega, 2001). Both methods are sensitive to spots, but the correlation method is also sensitive to amorphous features and large-scale structures that a human operator might ignore.

In our study, we record the position of each spot every 60 h and compute a velocity based on its displacement over this 60 h time interval. If the spot changes latitude by less than 1°, and if it changes velocity from the average value for its complete life history by less than 10 $\mathrm{m\,s^{-1}}$, then we will use the spot as a record for the wind velocity of the latitude in which it sits. In addition, for these latitudes in which there are few spots we use other features having stable nonoval shape as tracking targets to get the wind velocity for these latitudes. Then we average these records in different 1° bins to get the wind velocity for latitudes from 78° S to 83° N. This was impossible for some latitudes (77° N, 25° N, 21° N, 16° N, 10° N, 2° N–5° N, 1° S, 14° S, 26° S, 30° S, 37° S, 44° S, 54° S, 61° S, 63° S, 67° S–70° S and 77° S) where we could not find good tracking targets. We use interpolation to get the values of wind velocity at these latitudes.

Figure 7 shows that the wind profile obtained from Cassini by the feature tracking method is in good agreement with the wind profile obtained by the correlation method (Porco et al., 2003). The correlation coefficient between the two profiles from 78° S to 83° N is 0.9257. Porco et al. (2003) study changes in the jets from the Voyager time to the Cassini time. Further study of the changes of wind profiles requires a detailed discussion of the accuracy of data from different sources (Voyager, HST and Cassini) and an error analysis of velocity measurement in all these studies. Such an effort is beyond the scope of this study.

Using the data of Voyager, Ingersoll et al. (1979, 1981) and Limaye (1986) discussed the curvature of the westward jets and the jets' stability according to the barotropic stability criterion. In this paper, we repeat this work based on more data including Voyager, HST and Cassini. The Voyager data (Limaye, 1986) were taken in 1979. The HST data (Garcia-Melendo and Sanchez-Lavega, 2001) were taken from 1995 to 2000. The Cassini data were taken in 2000.

The barotropic stability criterion says that a two-dimensional (barotropic) flow is stable when $\beta - \bar{u}_{yy} > 0$ at all latitudes. Here $\beta = df/dy = 2\Omega\cos\phi/R_J$ is the planetary vorticity gradient, $f = 2\Omega\sin\phi$ is the Coriolis parameter, ϕ is planetographic latitude, Ω and R_J are Jupiter's angular rate of rotation and planetary radius, respectively; $\bar{u}$ is the mean zonal wind, y is the northward coordinate, and $\bar{u}_{yy}$ is the curvature of the jets. Since β is positive everywhere and $\bar{u}_{yy}$ is positive at the latitudes of the westward jets, the criterion is most likely to be violated at these latitudes. Vertical structure in the flow can alter its stability, but it is uncertain and we do not discuss it here.

Figure 8 shows parabolas with curvature β that are centered on the westward jets. The figure shows that some jets

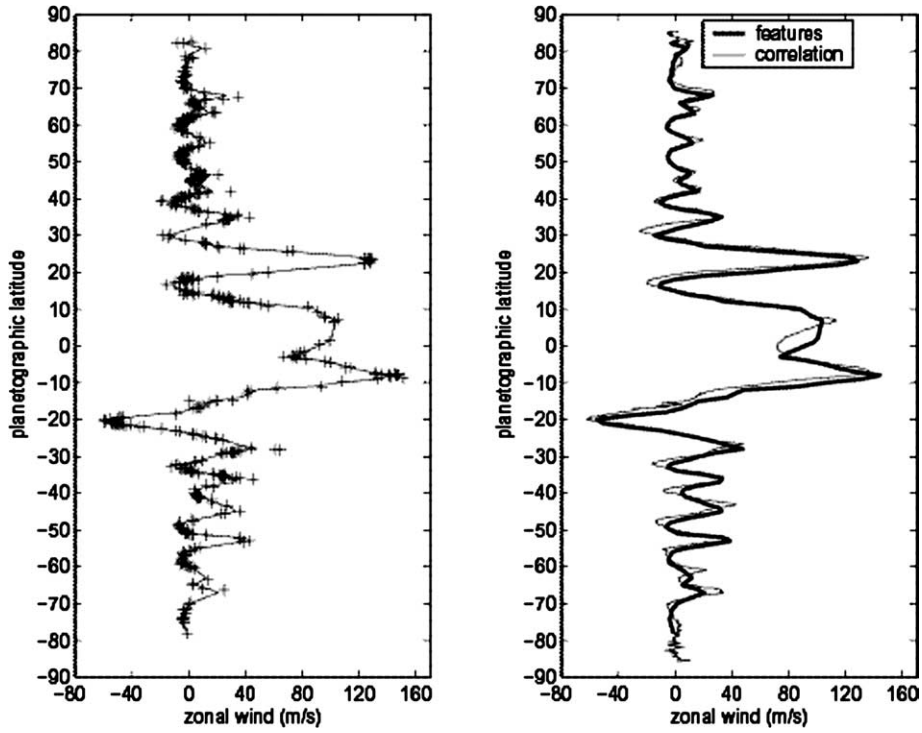

Fig. 7. The zonal wind profile obtained from Cassini by two different methods—feature tracking and correlation. Both wind profiles use planetographic latitudes. In the left panel, each point is a single feature, and the solid line is the average of the points in a 1° bin. In the right panel, the two lines are from feature tracking in this study and correlation method from Porco et al. (2003).

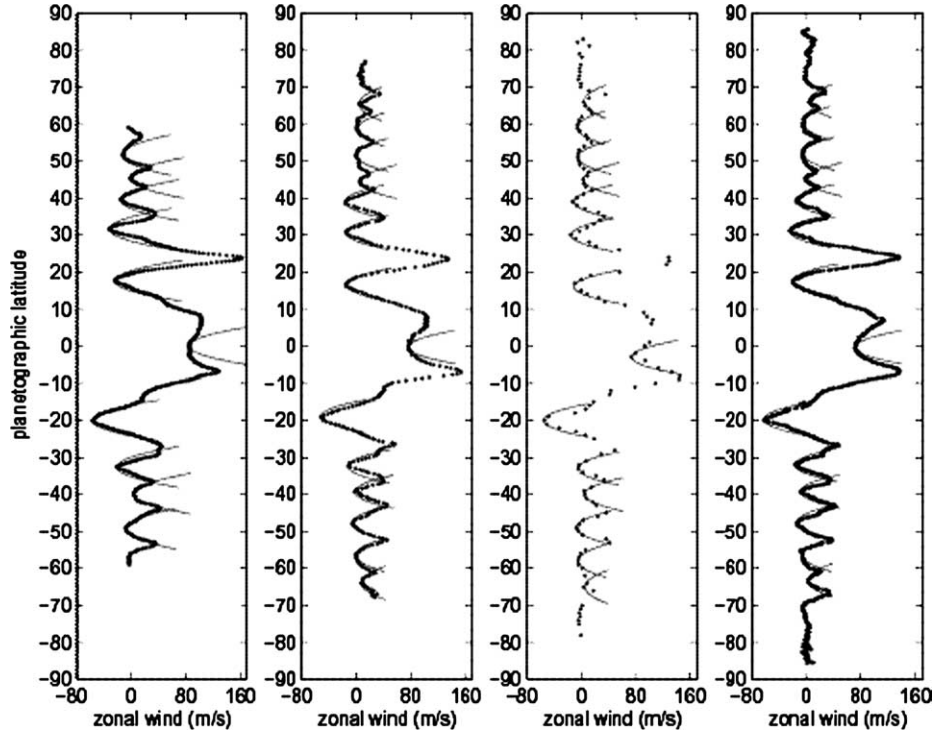

Fig. 8. Curvature $d^2\bar{u}/dy^2$ of the zonal velocity profile compared to β. From left to right the data are from Voyager (1979), HST (1995–2000), Cassini (2000) feature tracking, and Cassini correlation. The parabolic curves are defined by $d^2\bar{u}/dy^2 = \beta$, and are centered on the westward jet maxima. For the Cassini feature tracking profile, each point is an average of features in a 1° latitude bin. For the other profiles the resolution is 2–3 times better. Where the measured profile lies inside the parabola, the flow violates the barotropic stability criterion.

developed more curvature than β and others developed less curvature than β during the 21 years 1979–2000. The jet at 39° N had $\bar{u}_{yy} > \beta$ during HST time and less at other times. The jet at 31° N had $\bar{u}_{yy} > \beta$ during Voyager time and less at other times. The jet at 17° N had $\bar{u}_{yy} > \beta$ during Voyager times and less at other times. The jet at 20° S had $\bar{u}_{yy} > \beta$ during HST and Cassini times and less during Voyager times. The jet at 32° S had $\bar{u}_{yy} > \beta$ during Voyager time and less at other times. The general agreement between HST and Cassini and between the feature tracking and correlation methods suggests that the differences relative to β are significant. In general, the number of westward jets that clearly violate the barotropic stability criterion is about the same during Cassini time as during Voyager and HST times.

The left panel of Fig. 9 shows that in the northern hemisphere the spots are concentrated at the latitudes of the westward jets. The appearances and disappearances (not shown) of these compact spots have almost the same latitude distributions as the spots themselves. Since the westward jets are most likely to violate the barotropic stability criterion, they are most likely to develop waves and eddies, which could coalesce into spots (e.g., Dowling and Ingersoll, 1989). This may explain the distribution of spots in the northern hemisphere. However in the southern hemisphere there is not a good correlation between the latitude distribution of spots and zonal winds. Obviously, the barotropic stability criterion cannot explain the difference between the northern and southern hemispheres. Perhaps the GRS and the large White Oval Spot centered at −33° affect the distribution of spots in the southern hemisphere due to their large size.

The right panel of Fig. 9 shows that long-lived spots are concentrated at middle latitudes, mainly in anticyclonic bands. Their distribution is significantly different from that of all spots, which on average are concentrated in the westward jets (left panel of Fig. 9). Since the long-lived spots are anticyclonic, this observation is consistent with numerical models, which show that vortices of one sign are stable when they are imbedded in a region whose vorticity has the same sign (Ingersoll and Cuong, 1981; Williams and Yamagata, 1984; Marcus, 1988; Dowling and Ingersoll, 1989).

MJ found differences between the vortex speed and the mean zonal velocity at the central latitude of each vortex (see their Fig. 8). They found that the difference is anti-correlated with the mean zonal velocity. Figure 10 is the same as MJ Fig. 9, and shows the relative velocity (difference between the zonal velocity of the spot and that of the mean flow) vs the mean zonal velocity at the center of the spot. There is no obvious anti-correlation (negative slope) between the two variables, except possibly for the long-lived spots (bottom half) if one ignores the three points farthest to the right. The absolute value of the slope of the remaining points is less than that of the line in MJ Fig. 9. Our data in Fig. 10 are not too different from those in MJ Fig. 9, considering that their time base is much longer than ours and we have more data for short-lived spots (top half of Fig. 10).

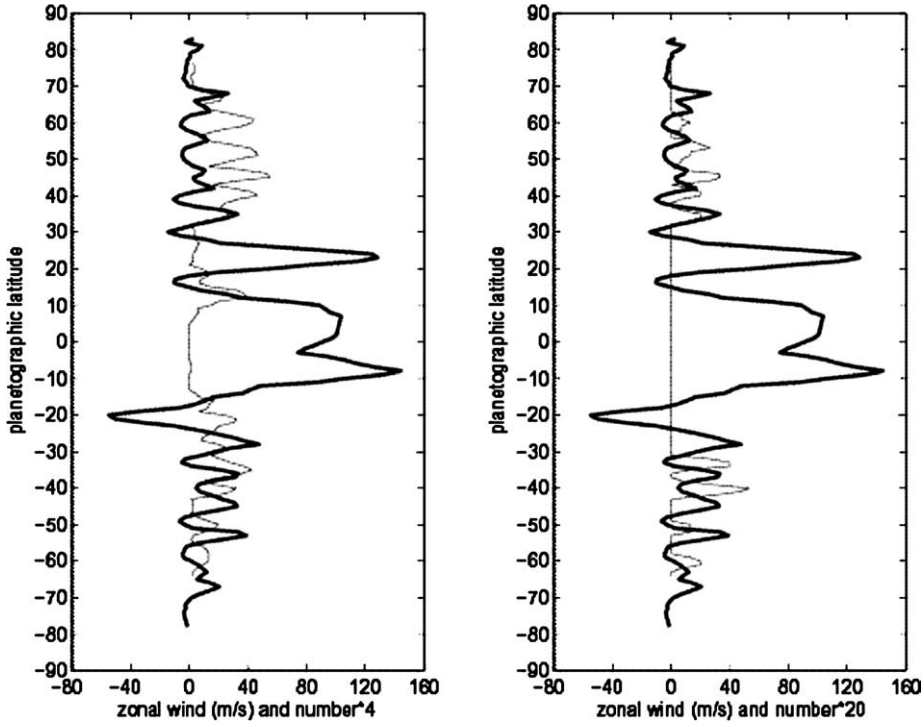

Fig. 9. Comparison between the latitude distribution of spots and the zonal wind profile. The left panel gives the number of all spots per degree of latitude with a scaling factor 4 (light line) along with the zonal wind profile determined by the feature tracking method (heavy line). The right panel is same as the left panel except for long-lived spots and scaling factor 20.

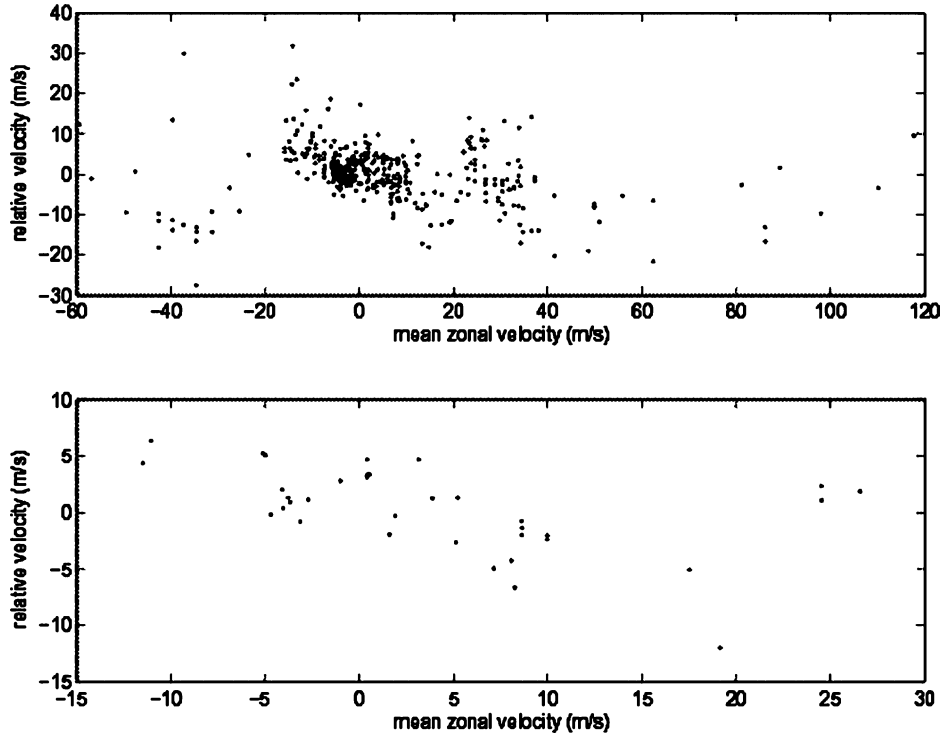

Fig. 10. Relative velocity (difference between the zonal velocity of the spot and that of the mean flow) vs mean zonal velocity. The mean zonal velocity is from Cassini (Porco et al., 2003). The top panel is for all spots, and the bottom panel is for long-lived spots. Each dot represents a spot. Compare with Fig. 9 of MJ.

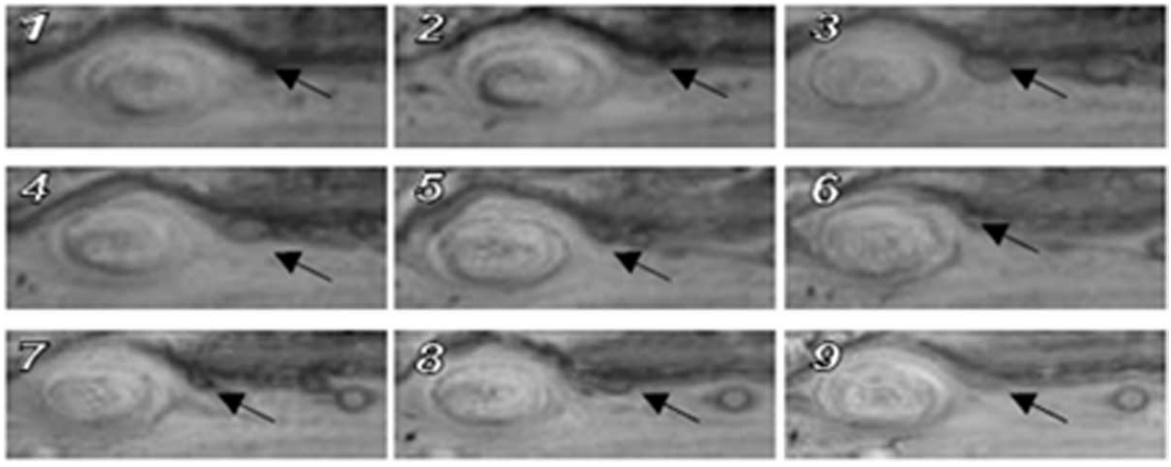

Fig. 11. Nine large spots absorbed by the GRS during the 70-day period. The range for every frame is (10° S–28° S, 130°–185°). This figure is not a time sequence like Figs. 2–4. Every subimage in this figure records a different large spot that will be absorbed by the GRS from the east at a different time.

6. Interaction with the GRS

As the largest anticyclone of the jovian atmosphere, the GRS has existed for at least 100 years and probably for over 300 years (Rogers, 1995). Smith et al. (1979) and Mac Low and Ingersoll (1986) recorded that the GRS absorbed smaller anticyclones, which suggests that the GRS maintains itself in this way (Ingersoll and Cuong, 1981; Ingersoll et al., 2000). Their conclusion is derived from Voyager observations, when the SEB was in one of its disturbed phases (labeled SEBD1 by Sanchez-Lavega and Gomez, 1996). During the Cassini encounter, from which our study was taken, the SEB was also in a disturbed phase. Our conclusions may not apply when the SEB is in its faded phase, as it was during the Pioneer 10 encounter in 1973.

During the 70-day period, we find nine large spots (major diameter greater than 2000 km) that were absorbed by the GRS from the east. These large spots are shown in Fig. 11. Further information about them is given in Table 2. In those cases where we could determine the vorticity (7 out of 9 cases), it was anticyclonic. In addition to these large spots, small dark spots were absorbed by the GRS from the

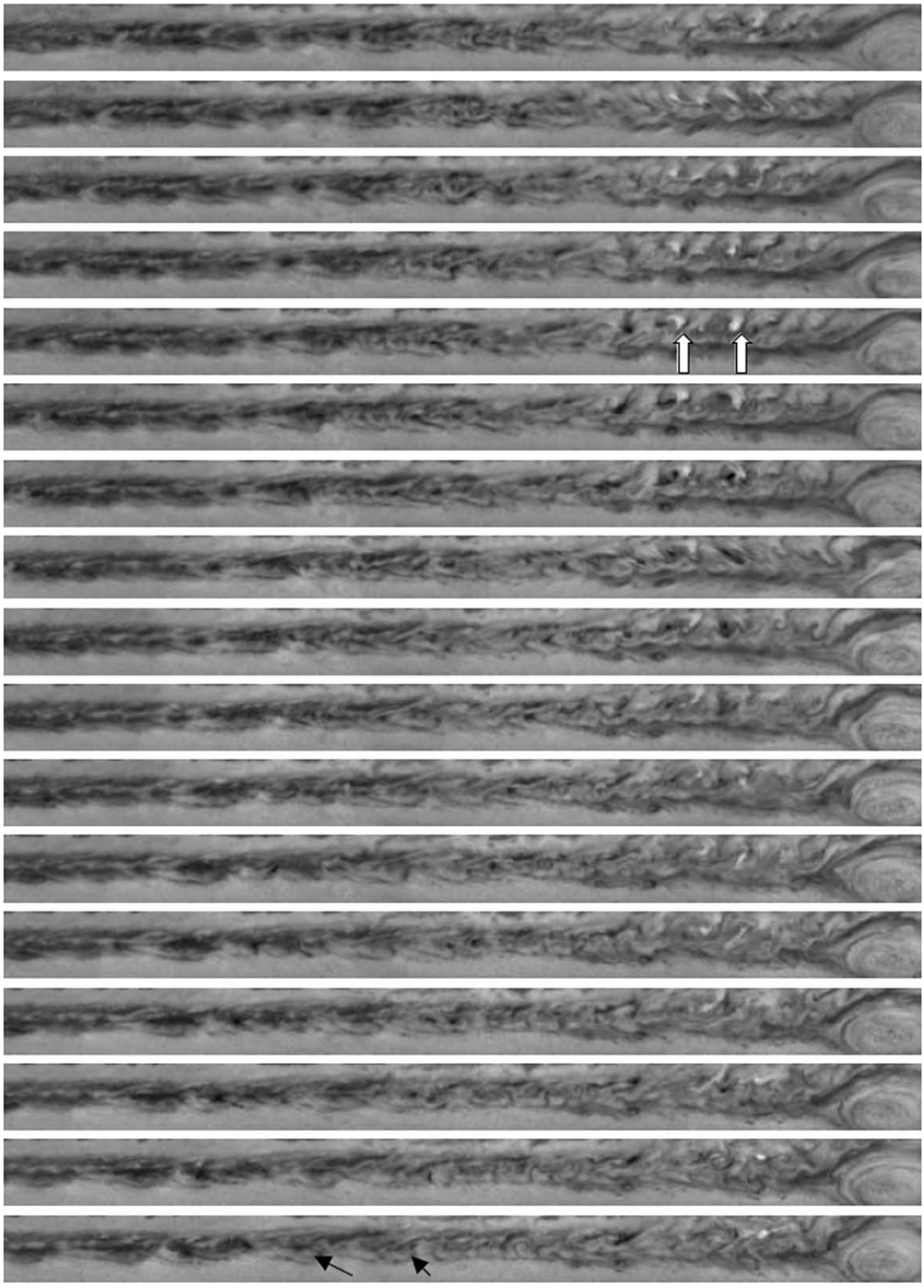

Fig. 12. Spots originating from the chaotic regions in the SEB west of the GRS. The range for every frame is (10° S–24° S, 320°–190°). Time increases down page 1 and then down page 2. The time of the first subimage is Nov 10, 2000. The time between two neighboring subimages is 20 h. Two examples of compact spots originating from the SEB and being absorbed finally by the GRS are shown with dark arrows. Tracing these spots from lower left to upper right (backwards in time), we find that all of them come from the chaotic regions in the SEB west of the GRS. In addition, two bright probable convective storms are shown with white arrows.

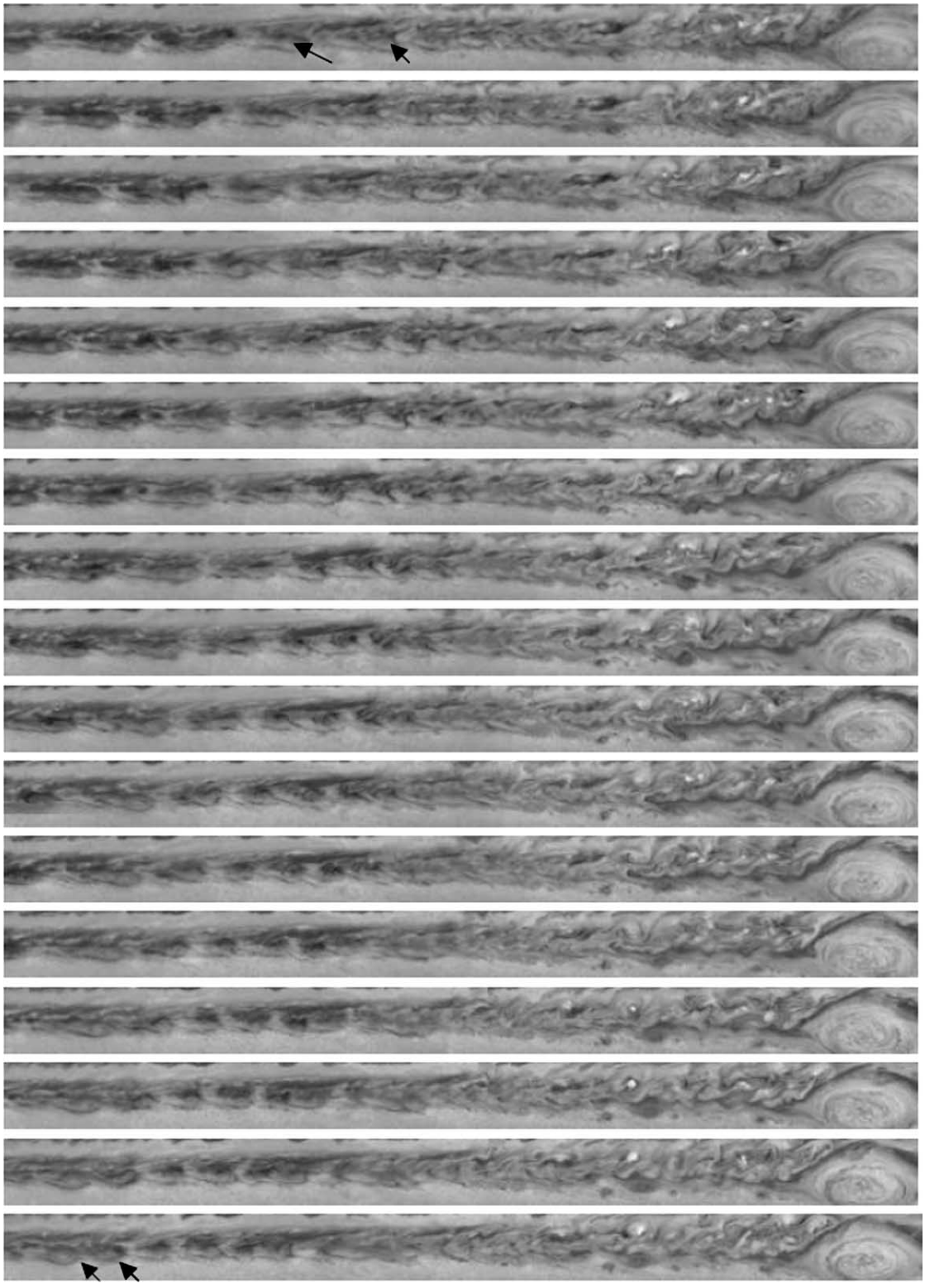

Fig. 12. (Continued.)

west. Because these spots are small and because we could not determine their vorticity, we have not included them in this discussion.

The large spots absorbed by the GRS probably originate from the CR's in the SEB west of the GRS. They are entrained into the westward jet to the south of the SEB and encounter the GRS from the east. Figure 12 shows a time history of spots coming from the chaotic regions in the SEB west of the GRS. Lightning observations (Gierasch et al., 2000) show that moist convection associated with convec-

Table 2
Nine spots absorbed by the GRS

Number	Time of absorbing	Long diameter (km)	Short diameter (km)	Vorticity
1	Oct 14 00:57	3513	1466	Anticyclone
2	Oct 18 14:37	5387	2053	Anticyclone
3	Nov 08 17:33	6675	2443	Unknown
4	Nov 12 14:37	5738	2443	Anticyclone
5	Nov 17 01:10	3513	1662	Anticyclone
6	Nov 17 21:02	2576	1173	Anticyclone
7	Nov 28 16:19	2928	1759	Unknown
8	Dec 02 20:02	3748	1759	Anticyclone
9	Dec 09 11:42	5270	2150	Anticyclone

tive storms is very active in the SEB west of the GRS. The last four subimages contain a probable convective storm that appears in Fig. 3 of Porco et al. (2003). Figure 12 also shows two other probable convective storms (white arrows) appearing in the same chaotic regions in the SEB. The fact that the westward-moving spots that are absorbed by the GRS originate in the same chaotic region as the probable convective storms suggests that development of westward-moving spots is related to the latent energy released by these storms. Some uncertainty remains, however, because there is no one-to-one correspondence between the compact spots and the convective storms (Fig. 12). They both originate in the same region, but they do not appear to be the same features.

Nevertheless, these observations support the idea that the chaotic regions in the SEB, probable convective storms, and the westward jet compose a system that supports the GRS (Gierasch et al., 2000; Ingersoll et al., 2000). In this system, convective storms in the SEB get energy from the interior of Jupiter by moist convection and deliver energy to the compact spots that will be absorbed by the GRS.

7. Conclusions

In this study, we record properties of over 500 spots during a 70-day period from the continuum band ISS images of Cassini. The relation between the spots and mean zonal wind profile and interactions between spots and the GRS are also discussed.

The appearance and disappearance of spots maintained a balance during the period, and the CR's are an important source and sink for spots. The major diameter of long-lived spots is greater than 2000 km.

Exponential functions provide a good fit to the distribution of lifetimes, with time constants of 3.5 days for probable convective storms and 16.8 days for all other spots.

Our wind profile from feature tracking is in good agreement with the one from the correlation method. The wind profile shows that the number of westward jets violating the barotropic stability criterion is about the same during Cassini time as during Voyager and HST times. The barotropic stability criterion can explain the observation that spots are concentrated at the latitudes of westward jets in the northern hemisphere, but the theory cannot explain why there is no such concentration in the southern hemisphere. The fact that long-lived spots are concentrated in anticyclonic bands is consistent with numerical models.

Spots that originate in the chaotic regions in the SEB are absorbed by the GRS. This and other observations suggest that the chaotic regions in the SEB, moist convection, the westward jet, and spots in the SEB latitudes compose a system supporting the GRS.

Acknowledgments

We wish to thank Mimi Gerstell, Shane Byrne, and Carol Shu for helpful suggestions on the technical aspects and English of this article. This work was supported by the Cassini Project and the Planetary Atmospheres Program of NASA.

References

Banfield, D., Gierasch, P.J., Bell, M., Ustinov, E., Ingersoll, A.P., Vasavada, A., Belton, M.J.S., 1998. Jupiter's cloud structure from Galileo imaging data. Icarus 135, 230–250.

Dowling, T.E., Ingersoll, A.P., 1989. Jupiter's Great Red Spot as a shallow water system. J. Atmos. Sci. 46, 3256–3278.

Garcia-Melendo, E., Sanchez-Lavega, A., 2001. A study of the stability of jovian zonal winds from HST images: 1995–2000. Icarus 152, 316–330.

Gierasch, P.J., Ingersoll, A.P., Banfield, D., Ewald, S.P., Helfenstein, P., Simon-Miller, A., Vasavada, A., Breneman, H.H., Senske, D.A., 2000. Observation of moist convection in Jupiter's atmosphere. Nature 403, 628–630.

Ingersoll, A.P., Cuong, P.-G., 1981. Numerical model of long-lived jovian vortices. J. Atmos. Sci. 38, 2067–2074.

Ingersoll, A.P., Beebe, R.F., Collins, S.A., Hunt, G.E., Mitchell, J.L., Muller, J.P., Smith, B.A., Terrile, R.J., 1979. Zonal velocity and texture in the jovian atmosphere inferred from Voyager images. Nature 280, 773–775.

Ingersoll, A.P., Beebe, R.F., Mitchell, J.L., Garneau, G.W., Yagi, G.M., Muller, J.P., 1981. Interaction of eddies and mean zonal flow on Jupiter as inferred from Voyager 1 and Voyager 2 Images. J. Geophys. Res. 86, 8733–8743.

Ingersoll, A.P., Gierasch, P.J., Banfield, D., Vasavada, A.R., 2000. Moist convection as an energy source for the large-scale motions in Jupiter's atmosphere. Nature 403, 630–632.

Limaye, S.S., 1986. New estimates of the mean zonal flow at the cloud level. Icarus 65, 335–352.

Little, B., Anger, C.D., Ingersoll, A.P., Vasavada, A.R., Senske, D.A., Breneman, H.H., Borucki, W.J., 1999. Galileo images of lightning on Jupiter. Icarus 142, 306–323.

Mac Low, M.-M., Ingersoll, A.P., 1986. Merging of vortices in the atmosphere of Jupiter: an analysis of Voyager images. Icarus 65, 353–369.

Marcus, P.S., 1988. Numerical simulation of Jupiter's Great Red Spot. Nature 331, 693–696.

Maxworthy, T., Redekopp, L.G., Weidman, P.D., 1978. On the production and interaction of planetary solitary waves: application to the jovian atmosphere. Icarus 33, 388–409.

Meyer, S.L., 1986. Data Analysis for Scientists and Engineers. Peer Management Consultants, Ltd., Evanston, pp. 74–75.

Mitchell, J.L., Terrile, R.J., Smith, B.A., Müller, J.P., Ingersoll, A.P., Hunt, G.E., Collins, S.A., Beebe, R.F., 1979. Jovian cloud structure and velocity fields. Nature 280, 776–778.

Morales-Juberias, R., Sanchez-Lavega, A., Lecacheux, J., Colas, F., 2002. A comparative study of jovian anticyclone properties from a six-year (1994–2000) survey. Icarus 157, 76–90.

Porco, C.C., 23 colleagues, 2003. Cassini imaging of Jupiter's atmosphere, satellites, and rings. Science 299, 1541–1547.

Rogers, J.H., 1995. The Giant Planet Jupiter. Cambridge Univ. Press, Cambridge, UK.

Sanchez-Lavega, A., Gomez, J.M., 1996. The South Equatorial Belt of Jupiter. I. Its life cycle. Icarus 121, 1–17.

Smith, B.A., Soderblom, L.A., Johnson, T.V., Ingersoll, A.P., Collins, S.A., Shoemaker, E.M., Hunt, G.E., Masursky, H., Carr, M.H., Davies, M.E., Cook II, A.F., Boyce, J., Danielson, G.E., Owen, T., Sagan, C., Beebe, R.F., Veverka, J., Strom, R.G., McCauley, J.F., Morrison, D., Briggs, G.A., Suomi, V.E., 1979. The Jupiter system through the eyes of Voyager 1. Science 204, 951–972.

Vasavada, A.R., Ingersoll, A.P., Banfield, D., Bell, M., Gierasch, P.J., Belton, M.J.S., Orton, G.S., Klaasen, K.P., De Jong, E., Breneman, H.H., Jones, T.J., Kaufman, J.M., Magee, K.P., Senske, D.A., 1998. Galileo imaging of Jupiter's atmosphere: the Great Red Spot, equatorial region, and White Ovals. Icarus 135, 265–275.

Williams, G.P., Yamagata, T., 1984. Geostrophic regimes, intermediate solitary vortices and jovian eddies. J. Atmos. Sci. 41, 453–478.

Youssef, A., Marcus, P.S., 2003. The dynamics of jovian white ovals from formation to merger. Icarus 162, 74–93.